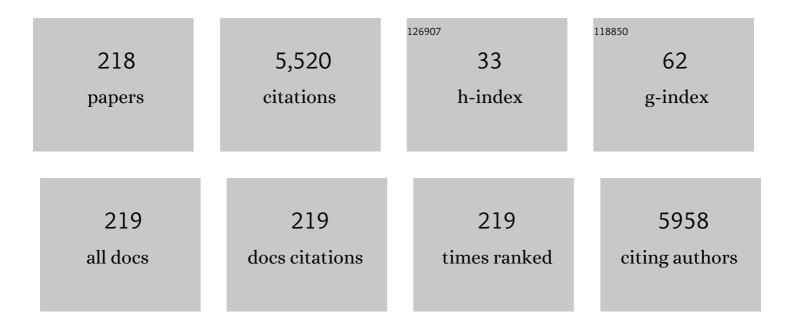
List of Publications by Year in descending order

Source: https://exaly.com/author-pdf/7746637/publications.pdf Version: 2024-02-01



KOSUKE NACASHIO

#	Article	IF	CITATIONS
1	Quantitative Determination of Contradictory Bandgap Values of Bulk PdSe ₂ from Electrical Transport Properties. Advanced Functional Materials, 2022, 32, 2108061.	14.9	11
2	Science of 2.5 dimensional materials: paradigm shift of materials science toward future social innovation. Science and Technology of Advanced Materials, 2022, 23, 275-299.	6.1	32
3	Performance Enhancement of SnS/ <i>h</i> -BN Heterostructure p-Type FET via the Thermodynamically Predicted Surface Oxide Conversion Method. ACS Applied Materials & Interfaces, 2022, 14, 19928-19937.	8.0	4
4	Ultrafast Operation of 2D Heterostructured Nonvolatile Memory Devices Provided by the Strong Short-Time Dielectric Breakdown Strength of <i>h</i> -BN. ACS Applied Materials & Interfaces, 2022, 14, 25659-25669.	8.0	4
5	Current Injection into Single-Crystalline Carbon-Doped <i>h</i> -BN toward Electronic and Optoelectronic Applications. ACS Applied Materials & Interfaces, 2022, 14, 25731-25740.	8.0	2
6	Quantization of Mode Shifts in Nanocavities Integrated with Atomically Thin Sheets. Advanced Optical Materials, 2022, 10, .	7.3	2
7	Ion conductive character of low-yttria-content yttria-stabilized zirconia at low temperature. Japanese Journal of Applied Physics, 2021, 60, SBBF03.	1.5	1
8	Material and Device Structure Designs for 2D Memory Devices Based on the Floating Gate Voltage Trajectory. ACS Nano, 2021, 15, 6658-6668.	14.6	16
9	All 2D Heterostructure Tunnel Field Effect Transistors. , 2021, , .		Ο
10	2D layered semiconductors: Challenge & Perspective. , 2021, , .		0
11	Intrinsic Electronic Transport Properties and Carrier Densities in PtS ₂ and SnSe ₂ : Exploration of n ⁺ â€Source for 2D Tunnel FETs. Advanced Electronic Materials, 2021, 7, 2100292.	5.1	8
12	Thermodynamic Perspective on the Oxidation of Layered Materials and Surface Oxide Amelioration in 2D Devices. ACS Applied Materials & Interfaces, 2021, 13, 43282-43289.	8.0	10
13	Thickness-dependent Raman active modes of SnS thin films. AIP Advances, 2021, 11, .	1.3	4
14	Atomic-Step-Induced Screw-Dislocation-Driven Spiral Growth of SnS. Chemistry of Materials, 2021, 33, 186-194.	6.7	16
15	Quantum-mechanical effect in atomically thin MoS 2 FET. 2D Materials, 2020, 7, 014001.	4.4	6
16	Understanding interface properties in 2D heterostructure FETs. Semiconductor Science and Technology, 2020, 35, 103003.	2.0	8
17	Micrometer-scale monolayer SnS growth by physical vapor deposition. Nanoscale, 2020, 12, 23274-23281.	5.6	21
18	All 2D Heterostructure Tunnel Field-Effect Transistors: Impact of Band Alignment and Heterointerface Quality. ACS Applied Materials & Interfaces, 2020, 12, 51598-51606.	8.0	35

#	ARTICLE Caulty Distribution Control in van der Waals Heterostructures of <mml:math< th=""><th>IF</th><th>CITATIONS</th></mml:math<>	IF	CITATIONS
19	xmlns:mml="http://www.w3.org/1998/Math/MathML" display="inline" overflow="scroll"> <mml:msub><mml:mrow><mml:mi>Mo</mml:mi><mml:mi mathvariant="normal">S</mml:mi </mml:mrow><mml:mn>2</mml:mn></mml:msub> and <mml:math <="" display="inline" td="" xmlns:mml="http://www.w3.org/1998/Math/MathML"><td>3.8</td><td>9</td></mml:math>	3.8	9
20	overflow="scroll"> <mml:msub>WS<mml:mn>2</mml:mn></mml:msub> Understanding the Memory Window Overestimation of 2D Materials Based Floating Gate Type Memory Devices by Measuring Floating Gate Voltage. Small, 2020, 16, e2004907.	10.0	11
21	Hexagonal Boron Nitride As an Ideal Substrate for Carbon Nanotube Photonics. ACS Photonics, 2020, 7, 1773-1779.	6.6	22
22	lsothermal Growth and Stacking Evolution in Highly Uniform Bernal-Stacked Bilayer Graphene. ACS Nano, 2020, 14, 6834-6844.	14.6	28
23	Purely in-plane ferroelectricity in monolayer SnS at room temperature. Nature Communications, 2020, 11, 2428.	12.8	214
24	Influence of Interlayer Stacking on Gate-Induced Carrier Accumulation in Bilayer MoS ₂ . ACS Applied Electronic Materials, 2020, 2, 1352-1357.	4.3	12
25	Full Energy Spectra of Interface State Densities for <i>n</i> ―and <i>p</i> â€type MoS ₂ Fieldâ€Effect Transistors. Advanced Functional Materials, 2019, 29, 1904465.	14.9	39
26	Interface engineering for 2D layered semiconductors. , 2019, , .		1
27	Influence of interface dipole layers on the performance of graphene field effect transistors. Carbon, 2019, 152, 680-687.	10.3	19
28	Detection of both optical polarization and coherence transfers to excitonic valley states in CVD-grown monolayer MoS ₂ . Applied Physics Express, 2019, 12, 063005.	2.4	5
29	Pinpoint pick-up and bubble-free assembly of 2D materials using PDMS/PMMA polymers with lens shapes. Applied Physics Express, 2019, 12, 055008.	2.4	33
30	Uniform and ultrathin high-κ gate dielectrics for two-dimensional electronic devices. Nature Electronics, 2019, 2, 563-571.	26.0	204
31	Expansion of the Graphdiyne Family: A Triphenylene-Cored Analogue. ACS Applied Materials & Interfaces, 2019, 11, 2730-2733.	8.0	58
32	Band tail interface states and quantum capacitance in a monolayer molybdenum disulfide field-effect-transistor. Journal Physics D: Applied Physics, 2018, 51, 065110.	2.8	30
33	Impact ionization and transport properties of hexagonal boron nitride in a constant-voltage measurement. Physical Review B, 2018, 97, .	3.2	15
34	Determination of Carrier Polarity in Fowler–Nordheim Tunneling and Evidence of Fermi Level Pinning at the Hexagonal Boron Nitride/Metal Interface. ACS Applied Materials & Interfaces, 2018, 10, 11732-11738.	8.0	25
35	Hydrogen-Assisted Epitaxial Growth of Monolayer Tungsten Disulfide and Seamless Grain Stitching. Chemistry of Materials, 2018, 30, 403-411.	6.7	60
36	Self-passivated ultra-thin SnS layers <i>via</i> mechanical exfoliation and post-oxidation. Nanoscale, 2018, 10, 22474-22483.	5.6	42

#	Article	IF	CITATIONS
37	Direct observation of electron capture and emission processes by the time domain charge pumping measurement of MoS2 FET. Applied Physics Letters, 2018, 113, .	3.3	11
38	Accumulation-Mode Two-Dimensional Field-Effect Transistor: Operation Mechanism and Thickness Scaling Rule. ACS Applied Materials & amp; Interfaces, 2018, 10, 32355-32364.	8.0	28
39	Type-II HfS ₂ /MoS ₂ Heterojunction Transistors. IEICE Transactions on Electronics, 2018, E101.C, 338-342.	0.6	6
40	2D Tunnel Field Effect Transistors (FETs) with a Stable Chargeâ€Transferâ€Type p ⁺ â€WSe ₂ Source. Advanced Electronic Materials, 2018, 4, 1800207.	5.1	41
41	Electrically Inert h-BN/Bilayer Graphene Interface in All-Two-Dimensional Heterostructure Field Effect Transistors. ACS Applied Materials & Interfaces, 2018, 10, 28780-28788.	8.0	24
42	Fabrication and Surface Engineering of Two-Dimensional SnS Toward Piezoelectric Nanogenerator Application. MRS Advances, 2018, 3, 2809-2814.	0.9	19
43	Crystalline Graphdiyne Nanosheets Produced at a Gas/Liquid or Liquid/Liquid Interface. Journal of the American Chemical Society, 2017, 139, 3145-3152.	13.7	438
44	Molecularly-thin anatase field-effect transistors fabricated through the solid state transformation of titania nanosheets. Nanoscale, 2017, 9, 6471-6477.	5.6	8
45	(Invited) Electrical Integrity and Anisotropy in Dielectric Breakdown of Layered h -BN Insulator. ECS Transactions, 2017, 79, 91-97.	0.5	1
46	Experimental detection of active defects in few layers MoS ₂ through random telegraphic signals analysis observed in its FET characteristics. 2D Materials, 2017, 4, 015035.	4.4	16
47	Graphene field-effect transistor application-electric band structure of graphene in transistor structure extracted from quantum capacitance. Journal of Materials Research, 2017, 32, 64-72.	2.6	8
48	Transport properties of the top and bottom surfaces in monolayer MoS ₂ grown by chemical vapor deposition. Nanoscale, 2017, 9, 13264-13271.	5.6	18
49	Buffer layer engineering on graphene via various oxidation methods for atomic layer deposition. Applied Physics Express, 2016, 9, 125101.	2.4	18
50	Comparison of device structures for the dielectric breakdown measurement of hexagonal boron nitride. Applied Physics Letters, 2016, 109, .	3.3	15
51	Anisotropic Dielectric Breakdown Strength of Single Crystal Hexagonal Boron Nitride. ACS Applied Materials & Interfaces, 2016, 8, 27877-27884.	8.0	53
52	Metal Contacts to Graphene. Series in Materials Science and Engineering, 2016, , 53-78.	0.1	1
53	Dielectric breakdown of layered insulator. , 2016, , .		0
54	Gap state analysis in electric-field-induced band gap for bilayer graphene. Scientific Reports, 2015, 5, 15789.	3.3	36

#	Article	IF	CITATIONS
55	Subthreshold transport in mono- and multilayered MoS ₂ FETs. Applied Physics Express, 2015, 8, 065203.	2.4	12
56	Recent progress of junction technology for germanium CMOS. , 2015, , .		0
57	Atomic layer deposition of Y ₂ O ₃ on <i>h</i> BN for a gate stack in graphene FETs. Nanotechnology, 2015, 26, 175708.	2.6	13
58	Layer-by-Layer Dielectric Breakdown of Hexagonal Boron Nitride. ACS Nano, 2015, 9, 916-921.	14.6	174
59	Reliability assessment of germanium gate stacks with promising initial characteristics. Applied Physics Express, 2015, 8, 021301.	2.4	7
60	Fully dry PMMA transfer of graphene on <i>h</i> -BN using a heating/cooling system. 2D Materials, 2015, 2, 041002.	4.4	116
61	Graphene/Metal Contact. , 2015, , 53-78.		4
62	Thermally robust CMOS-aware Ge MOSFETs with high mobility at high-carrier densities on a single orientation Ge substrate. , 2014, , .		12
63	(Invited) Quantum Capacitance Measurement of Bilayer Graphene. ECS Transactions, 2014, 61, 75-80.	0.5	1
64	Kinetic model for scavenging of SiO <inf>2</inf> interface layer in HfO <inf>2</inf> gate stacks. , 2014, , .		1
65	Enhancement of thermal stability and water resistance in yttrium-doped GeO ₂ /Ge gate stack. Applied Physics Letters, 2014, 104, 092909.	3.3	34
66	Effect of Si substrate on interfacial SiO2 scavenging in HfO2/SiO2/Si stacks. Applied Physics Letters, 2014, 105, .	3.3	14
67	The crystal orientation relation and macroscopic surface roughness in hetero-epitaxial graphene grown on Cu/mica. Nanotechnology, 2014, 25, 185602.	2.6	12
68	Structural and thermodynamic consideration of metal oxide doped GeO2 for gate stack formation on germanium. Journal of Applied Physics, 2014, 116, .	2.5	33
69	Atomically flat planarization of Ge(100), (110), and (111) surfaces in H ₂ annealing. Applied Physics Express, 2014, 7, 051301.	2.4	12
70	Analytical Formulation of SiO <inf>2</inf> -IL scavenging in HfO <inf>2</inf> /SiO <inf>2</inf> /Si gate stacks - A key is the SiO <inf>2</inf> /Si interface reaction. , 2014, , .		2
71	(Invited) Significant Enhancement of High-Ns Electron Mobility in Ge n-MOSFETs with Atomically Flat Ge/GeO2 Interface. ECS Transactions, 2014, 61, 147-156.	0.5	4
72	Impacts of oxygen passivation on poly-crystalline germanium thin film transistor. Thin Solid Films, 2014, 557, 334-337.	1.8	47

#	Article	IF	CITATIONS
73	Large Fermi energy modulation in graphene transistors with high-pressure O ₂ -annealed Y ₂ O ₃ topgate insulators. Applied Physics Letters, 2014, 104, 083519.	3.3	18
74	Atomic-scale planarization of Ge (111), (110) and (100) surfaces. , 2014, , .		0
75	HfO2-assisted SiO2 reduction in HfO2/SiO2/Si stacks. Thin Solid Films, 2014, 557, 272-275.	1.8	7
76	Orbital-specific Tunability of Many-Body Effects in Bilayer Graphene by Gate Bias and Metal Contact. Scientific Reports, 2014, 4, 3713.	3.3	28
77	The density of states of graphene underneath a metal electrode and its correlation with the contact resistivity. Applied Physics Letters, 2013, 103, 033514.	3.3	34
78	Estimation of residual carrier density near the Dirac point in graphene through quantum capacitance measurement. Applied Physics Letters, 2013, 102, .	3.3	35
79	Carrier density modulation in graphene underneath Ni electrode. Journal of Applied Physics, 2013, 114, 024503.	2.5	17
80	Oxygen potential engineering of interfacial layer for deep sub-nm EOT high-k gate stacks on Ge. , 2013, ,		24
81	High electron mobility (>16 cm⁢sup>2⁢/sup>/V⁢inf>sec⁢/inf>) FETs with high on/off ratio (>10 ⁶) and highly conductive films (σ>10 ² S/cm) by chemical doping in very thin (∼20 nm) TiO <inf>2</inf> films on thermally grown SiO <inf>2</inf> .,		2
82	Reconsideration of electron mobility in Ge n-MOSFETs from Ge substrate side — Atomically flat surface formation, layer-by-layer oxidation, and dissolved oxygen extraction. , 2013, , .		10
83	Direct observation of charge transfer region at interfaces in graphene devices. Applied Physics Letters, 2013, 102, .	3.3	33
84	Conduction band offset at GeO2/Ge interface determined by internal photoemission and charge-corrected x-ray photoelectron spectroscopies. Applied Physics Letters, 2013, 102, .	3.3	29
85	Characterization of electron mobility in ultrathin body germanium-on-insulator metal-insulator-semiconductor field-effect transistors. Applied Physics Letters, 2013, 102, .	3.3	35
86	Quantitative Characterization of Band-Edge Energy Positions in High-kDielectrics by X-ray Photoelectron Spectroscopy. Japanese Journal of Applied Physics, 2013, 52, 021101.	1.5	4
87	(Invited) Graphene Underneath Metals. ECS Transactions, 2013, 53, 71-79.	0.5	1
88	High Electron Mobility in Germanium Junctionless n-MOSFETs. ECS Transactions, 2013, 58, 309-315.	0.5	4
89	Investigations on GeO Disproportionation Using X-ray Photoelectron Spectroscopy. ECS Transactions, 2013, 50, 557-567.	0.5	2
90	Atomically Flat Germanium (111) Surface by Hydrogen Annealing. ECS Transactions, 2013, 58, 201-206.	0.5	2

#	Article	IF	CITATIONS
91	Carrier response in band gap and multiband transport in bilayer graphene under the ultra-high displacement. , 2013, , .		0
92	Conduction Band-Offset in GeO2/Ge Stack Determined by Internal Photoemission Spectroscopy. ECS Transactions, 2013, 50, 91-95.	0.5	3
93	Interface Dipole Cancellation in SiO2/High-k/SiO2/Si Gate Stacks. ECS Transactions, 2013, 50, 159-163.	0.5	2
94	Step and Terrace Formation on Ge(111) Surface in H\$_{2}\$ Annealing. Applied Physics Express, 2012, 5, 121301.	2.4	10
95	Experimental and Analytical Characterization of Dual-Gated Germanium Junctionless p-Channel Metal–Oxide–Semiconductor Field-Effect Transistors. Japanese Journal of Applied Physics, 2012, 51, 04DA03.	1.5	7
96	Counter Dipole Layer Formation in Multilayer High-\$k\$ Gate Stacks. Japanese Journal of Applied Physics, 2012, 51, 081303.	1.5	13
97	Effect of High-Pressure Inert Gas Annealing on AlON/Ge Gate Stacks. Applied Physics Express, 2012, 5, 091002.	2.4	3
98	Variation of Surface Roughness on Ge Substrate by Cleaning in Deionized Water and its Influence on Electrical Properties in Ge Metal–Oxide–Semiconductor Field-Effect Transistors. Japanese Journal of Applied Physics, 2012, 51, 104203.	1.5	1
99	Oxidation Rate Reduction of Ge with O\$_{2}\$ Pressure Increase. Applied Physics Express, 2012, 5, 114001.	2.4	12
100	Understanding ^ ^amp; Controlling the Graphene/SiO2 Interaction. Hyomen Kagaku, 2012, 33, 552-556.	0.0	0
101	Counter dipole layer formation in SiO <inf>2</inf> /high-k/SiO <inf>2</inf> /Si gate stacks. , 2012, , .		0
102	Intrinsic graphene/metal contact. , 2012, , .		9
103	Recent Progress of Germanium Gate Stack Technology. , 2012, , .		0
104	Real-time x-ray diffraction of metastable phases during solidification from the undercooled LuFeO3 melt by two-dimensional detector at 1 kHz. Applied Physics Letters, 2012, 100, 191905.	3.3	4
105	Experimental and Analytical Characterization of Dual-Gated Germanium Junctionless p-Channel Metal–Oxide–Semiconductor Field-Effect Transistors. Japanese Journal of Applied Physics, 2012, 51, 04DA03.	1.5	15
106	Counter Dipole Layer Formation in Multilayer High-kGate Stacks. Japanese Journal of Applied Physics, 2012, 51, 081303.	1.5	0
107	Variation of Surface Roughness on Ge Substrate by Cleaning in Deionized Water and its Influence on Electrical Properties in Ge Metal–Oxide–Semiconductor Field-Effect Transistors. Japanese Journal of Applied Physics, 2012, 51, 104203.	1.5	1
108	Experimental study of carrier transport in ultra-thin body GeOI MOSFETs. , 2011, , .		14

#	Article	IF	CITATIONS
109	High-Electron-Mobility Ge n-Channel Metal–Oxide–Semiconductor Field-Effect Transistors with High-Pressure Oxidized Y ₂ O ₃ . Applied Physics Express, 2011, 4, 064201.	2.4	73
110	Electrical transport properties of graphene on SiO2 with specific surface structures. Journal of Applied Physics, 2011, 110, .	2.5	167
111	Is graphene contacting with metal still graphene?. , 2011, , .		2
112	High-Electron-Mobility \$hbox{Ge/GeO}_{2}\$ n-MOSFETs With Two-Step Oxidation. IEEE Transactions on Electron Devices, 2011, 58, 1295-1301.	3.0	118
113	Isotope Tracing Study of GeO Desorption Mechanism from GeO ₂ /Ge Stack Using ⁷³ Ge and ¹⁸ O. Japanese Journal of Applied Physics, 2011, 50, 04DA01.	1.5	19
114	Interfacial Dipole at High-k Dielectric/SiO ₂ Interface: X-ray Photoelectron Spectroscopy Characteristics. Japanese Journal of Applied Physics, 2011, 50, 031502.	1.5	10
115	Kinetic Effects of O-Vacancy Generated by GeO\$_{2}/Ge Interfacial Reaction. Japanese Journal of Applied Physics, 2011, 50, 10PE04.	1.5	4
116	Material potential and scalability challenges of germanium CMOS. , 2011, , .		40
117	Junctionless Ge p-Channel Metal–Oxide–Semiconductor Field-Effect Transistors Fabricated on Ultrathin Ge-on-Insulator Substrate. Applied Physics Express, 2011, 4, 031302.	2.4	39
118	Junctionless Ge MOSFETs Fabricated on 10 nm-Thick GeOI Substrate. ECS Transactions, 2011, 35, 457-464.	0.5	3
119	Density-of-States Limited Contact Resistance in Graphene Field-Effect Transistors. Japanese Journal of Applied Physics, 2011, 50, 070108.	1.5	44
120	Recent Progress of Ge Technology for a Post-Si CMOS. ECS Transactions, 2011, 35, 443-456.	0.5	7
121	Interfacial Dipole at High-kDielectric/SiO2Interface: X-ray Photoelectron Spectroscopy Characteristics. Japanese Journal of Applied Physics, 2011, 50, 031502.	1.5	10
122	lsotope Tracing Study of GeO Desorption Mechanism from GeO ₂ /Ge Stack Using ⁷³ Ge and ¹⁸ O. Japanese Journal of Applied Physics, 2011, 50, 04DA01.	1.5	22
123	Density-of-States Limited Contact Resistance in Graphene Field-Effect Transistors. Japanese Journal of Applied Physics, 2011, 50, 070108.	1.5	76
124	Kinetic Effects of O-Vacancy Generated by GeO ₂ /Ge Interfacial Reaction. Japanese Journal of Applied Physics, 2011, 50, 10PE04.	1.5	13
125	Desorption kinetics of GeO from GeO2/Ge structure. Journal of Applied Physics, 2010, 108, .	2.5	112
126	(Invited) Formation of Dipole Layers at Oxide Interfaces in High-k Gate Stacks. ECS Transactions, 2010, 33, 463-477.	0.5	9

#	Article	IF	CITATIONS
127	Resistive Switching Behaviors of NiO Bilayer Films with Different Crystallinity Layers. ECS Transactions, 2010, 28, 315-322.	0.5	4
128	(Invited) Oxidation, Diffusion and Desorption in a Ge/GeO ₂ System. ECS Transactions, 2010, 28, 171-180.	0.5	18
129	Systematic Investigation of the Intrinsic Channel Properties and Contact Resistance of Monolayer and Multilayer Graphene Field-Effect Transistor. Japanese Journal of Applied Physics, 2010, 49, 051304.	1.5	100
130	(Invited) Feasibility of Ge CMOS for Beyond Si-CMOS. ECS Transactions, 2010, 33, 33-46.	0.5	3
131	Impacts of graphene/SiO <inf>2</inf> interaction on FET mobility and Raman spectra in mechanically exfoliated graphene films. , 2010, , .		7
132	Observation of Dipole Layer Formed at High- <i>k</i> Dielectrics/SiO ₂ Interface with X-ray Photoelectron Spectroscopy. Applied Physics Express, 2010, 3, 061501.	2.4	19
133	Long range pinning interaction in ultra-thin insulator-inserted metal/germanium junctions. , 2010, , .		4
134	Ge MOSFETs performance: Impact of Ge interface passivation. , 2010, , .		63
135	Experimental Demonstration of Higher-k Phase HfO ₂ Through Non-Equilibrium Thermal Treatment. ECS Transactions, 2010, 28, 203-212.	0.5	18
136	Contact resistivity and current flow path at metal/graphene contact. Applied Physics Letters, 2010, 97, .	3.3	282
137	Electron mobility in high-k Ge-MISFETs goes up to higher. , 2010, , .		8
138	Control of Properties of GeO2 Films and Ge/GeO2 Interfaces by the Suppression of GeO Volatilization. ECS Transactions, 2009, 19, 101-116.	0.5	17
139	Thermodynamics and Kinetics for Suppression of GeO Desorption by High Pressure Oxidation of Ge. Materials Research Society Symposia Proceedings, 2009, 1155, 1.	0.1	13
140	Ge/GeO2 Interface Control with High Pressure Oxidation for Improving Electrical Characteristics. ECS Transactions, 2009, 19, 165-173.	0.5	24
141	Opportunities and challenges for Ge CMOS – Control of interfacing field on Ge is a key (Invited) Tj ETQq1 1 0	.784314 rg 2.4	$_{135}^{\rm gBT}$ /Overlock
142	Grain size increase in pentacene thin films prepared in low-pressure gas ambient. Thin Solid Films, 2009, 518, 507-509.	1.8	1
143	Spherical crystallization of Si during free fall in drop-tubes. Journal of Crystal Growth, 2009, 311, 722-726.	1.5	9
144	Metal/graphene contact as a performance Killer of ultra-high mobility graphene analysis of intrinsic mobility and contact resistance. , 2009, , .		86

#	Article	IF	CITATIONS
145	Comprehensive study of GeO <inf>2</inf> oxidation, GeO desorption and GeO <inf>2</inf> -metal interaction -understanding of Ge processing kinetics for perfect interface control , 2009, , .		10
146	Record-high electron mobility in Ge n-MOSFETs exceeding Si universality. , 2009, , .		57
147	Crystal Growth of Spherical Si. Advances in Materials Research, 2009, , 121-134.	0.2	1
148	Spreading and solidification of a highly undercooled Y3Al5O12 droplet impinging on a substrate. International Journal of Heat and Mass Transfer, 2008, 51, 2455-2461.	4.8	4
149	Orientation Analysis of Hexagonal Dendrite Formed from an Undercooled Melt of α-Fe2Si5. Metallurgical and Materials Transactions A: Physical Metallurgy and Materials Science, 2008, 39, 135-141.	2.2	2
150	Microstructure formation and in situ phase identification from undercooled Co–61.8at.% Si melts solidified on an electromagnetic levitator and an electrostatic levitator. Acta Materialia, 2008, 56, 2514-2525.	7.9	22
151	Formation of Hexagonal Metastable Phases from an Undercooled LuFeO3Melt in an Atmosphere with Low Oxygen Partial Pressure. Journal of the American Ceramic Society, 2008, 91, 806-812.	3.8	29
152	An investigation of the phase diagram of the Al–Ir binary system. Intermetallics, 2008, 16, 1171-1178.	3.9	18
153	ä¼źŽã,³ã,¹ãƒ^・çœè³‡æºã,'実ç¾ãĩMã,‹å¤™½é›»æ±ç"¨Siç∮çŠ¶çµæ™¶ã®è,²æˆ; Materia Japan, 2008, 47, 147-	1561	2
154	Study of Kinetic Behaviors of GeO in GeO2/Ge Stacks. ECS Transactions, 2008, 16, 187-194.	0.5	8
155	Nucleation of Cubic Phase in Deeply Undercooled Melt of Anisotropic Material. Transactions of the Materials Research Society of Japan, 2008, 33, 385-388.	0.2	0
156	Dynamic process of dendrite fragmentation in solidification from undercooled Si melt using time-resolved x-ray diffraction. Applied Physics Letters, 2007, 91, 061916.	3.3	8
157	Direct observation of the melt/substrate interface in melt spinning. Materials Science & Engineering A: Structural Materials: Properties, Microstructure and Processing, 2007, 449-451, 1033-1035.	5.6	2
158	Novel criterion for formation of metastable phase from undercooled melt. Materials Science & Engineering A: Structural Materials: Properties, Microstructure and Processing, 2007, 449-451, 675-679.	5.6	16
159	Microtexture formation of Ni99B1 alloys solidified on an ESL and an EML—a study based on the EBSP technique. Materials Science & Engineering A: Structural Materials: Properties, Microstructure and Processing, 2007, 449-451, 684-688.	5.6	1
160	In Situ Observation of Metastable Rare-Earth Iron Garnet Formed at the Melt/Substrate Interface by Splat Quenching. Journal of the American Ceramic Society, 2007, 90, 238-243.	3.8	4
161	Density and Thermal Conductivity Measurements for Silicon Melt by Electromagnetic Levitation under a Static Magnetic Field. International Journal of Thermophysics, 2007, 28, 44-59.	2.1	32
162	急冷å‡å›ºéŽç∵‹ã®å•視化ã,'目指ã⊷ã┥. Materia Japan, 2006, 45, 294-297.	0.1	1

#	Article	IF	CITATIONS
163	Formation of Metastable Rare-Earth Iron Garnet by Splat Quenching. Journal of the American Ceramic Society, 2006, 89, 1504-1509.	3.8	6
164	Experimental verification of ribbon formation process in chill-block melt spinning. Acta Materialia, 2006, 54, 2353-2360.	7.9	10
165	A comparative EBSP study of microstructure and microtexture formation from undercooled Ni99B1 melts solidified on an electrostatic levitator and an electromagnetic levitator. Acta Materialia, 2006, 54, 3791-3799.	7.9	26
166	Structural change in silicon from undercooled liquid state to crystalline state during crystallization. Journal of Crystal Growth, 2006, 294, 16-21.	1.5	7
167	Spherical Silicon Crystal Formed by Semisolid Process in Drop Tube. Japanese Journal of Applied Physics, 2006, 45, L623-L626.	1.5	26
168	Correlation of the electrical and optical properties of p-type CdGeAs2. Journal of Applied Physics, 2006, 99, 013512.	2.5	8
169	Real-time x-ray observation of solidification from undercooled Si melt. Journal of Applied Physics, 2006, 100, 033524.	2.5	15
170	In situ identification of the metastable phase during solidification from the undercooled YFeO3 melt by fast x-ray diffractometry at 250Hz. Applied Physics Letters, 2006, 89, 241923.	3.3	24
171	Optical absorption issues in CdGeAs 2 single crystals. , 2005, , .		0
172	In situ observation of solidification behavior of Si melt dropped on Si wafer by IR thermography. Journal of Crystal Growth, 2005, 275, e1685-e1690.	1.5	12
173	Microtexture and macrotexture formation in the containerless solidification of undercooled Ni–18.7 at.% Sn eutectic melts. Acta Materialia, 2005, 53, 731-741.	7.9	34
174	Growth mechanism of twin-related and twin-free facet Si dendrites. Acta Materialia, 2005, 53, 3021-3029.	7.9	115
175	Fragmentation of faceted dendrite in solidification of undercooled B-doped Si melts. Metallurgical and Materials Transactions A: Physical Metallurgy and Materials Science, 2005, 36, 3407-3413.	2.2	14
176	Experimental evidence of crystal fragmentation from highly undercooled Ni99B1 melts processed on an electrostatic levitator. Metallurgical and Materials Transactions A: Physical Metallurgy and Materials Science, 2005, 36, 3254-3257.	2.2	11
177	Photoluminescence of n-type CdGeAs2. Journal of Physics Condensed Matter, 2005, 17, 5687-5696.	1.8	3
178	Urbach rule used to explain the variation of the absorption edge in CdGeAs2crystals. Journal of Physics Condensed Matter, 2005, 17, 549-558.	1.8	10
179	Luminescence and optical absorption study of p-type CdGeAs2. Journal of Physics Condensed Matter, 2004, 16, 1279-1286.	1.8	16
180	Donor-acceptor pair emission near 0.55 eV in CdGeAs2. Journal of Applied Physics, 2004, 95, 4840-4844.	2.5	15

#	Article	IF	CITATIONS
181	Fiber growth of near stoichiometric LiNbO3 single crystals by the laser-heated pedestal growth method. Journal of Crystal Growth, 2004, 265, 190-197.	1.5	10
182	Correlation between dislocation etch pits and optical absorption in CdGeAs2. Journal of Crystal Growth, 2004, 269, 195-206.	1.5	16
183	Containerless solidification of undercooled oxide and metallic eutectic melts. Materials Science & Engineering A: Structural Materials: Properties, Microstructure and Processing, 2004, 375-377, 528-533.	5.6	10
184	Spreading and solidification behavior of molten Si droplets impinging on substrates. Acta Materialia, 2004, 52, 5295-5301.	7.9	18
185	Effect of donors and acceptors on the optical properties of CdGeAs2. , 2004, , .		Ο
186	Phase Selection in Undercooled Y ₃ Al ₅ O ₁₂ Melt. Materials Transactions, 2004, 45, 2723-2727.	1.2	11
187	Containerless solidification of highly undercooled Al2O3–ZrO2 eutectic melts on an aero-acoustic levitator. Journal of Crystal Growth, 2003, 249, 625-633.	1.5	16
188	Formation of YxNd1â^'xBa2Cu3O7â^'δ (0â‰ ¤ â‰ 0 .9) superconductors from an undercooled melt via aero–acoustic levitation. Materials Science & Engineering A: Structural Materials: Properties, Microstructure and Processing, 2003, 341, 1-8.	5.6	9
189	Electron paramagnetic resonance of Cr[sup 2+] and Cr[sup 4+] ions in CdGeAs[sub 2] crystals. Journal of Applied Physics, 2003, 94, 7567.	2.5	16
190	Nucleation behaviour and anomalous eutectic formation in highly undercooled Fe2O3-La2O3eutectic melts. Philosophical Magazine, 2003, 83, 1095-1109.	1.6	11
191	Containerless Solidification and Net Shaping by Splat Quenching of Undercooled Nd ₂ Fe ₁₄ B Melts. Materials Transactions, 2003, 44, 853-860.	1.2	8
192	Microstructure formation and phase selection in the solidification of Al2O3–5 at% SiO2 melts by splat quenching. Journal of Materials Research, 2002, 17, 2026-2032.	2.6	4
193	Phase selection in containerless solidification of Y3Al5O12. , 2002, , .		1
194	Containerless solidification of undercooled mullite - Crystallization, microstructure and phase selection. , 2002, , .		0
195	On the origin of recalescence behaviors of undercooled single-phase mullite and double-phase Al2O3–ZrO2 eutectic melts. Scripta Materialia, 2002, 47, 213-218.	5.2	18
196	Direct observation of the crystal-growth transition in undercooled silicon. Metallurgical and Materials Transactions A: Physical Metallurgy and Materials Science, 2002, 33, 2947-2953.	2.2	30
197	Microstructure of Y3Al5O12 garnet solidified from the melt undercooled beyond the hypercooling limit. Metallurgical and Materials Transactions A: Physical Metallurgy and Materials Science, 2002, 33, 2955-2961.	2.2	3
198	Containerless solidification of highly undercooled mullite melts: Crystal growth behavior and microstructure formation. Metallurgical and Materials Transactions A: Physical Metallurgy and Materials Science, 2002, 33, 2677-2683.	2.2	6

#	Article	IF	CITATIONS
199	Phase selection in the undercooled peritectic Y3Fe5O12 melt. Acta Materialia, 2002, 50, 1973-1981.	7.9	24
200	Reexamination of the solidification behavior of undercooled Ni–Sn eutectic melts. Acta Materialia, 2002, 50, 3241-3252.	7.9	23
201	Spherical Yttrium Aluminum Garnet Embedded in a Glass Matrix. Journal of the American Ceramic Society, 2002, 85, 2353-2358.	3.8	27
202	Metastable Phase Formation from an Undercooled Rare-Earth Orthoferrite Melt. Journal of the American Ceramic Society, 2002, 85, 2550-2556.	3.8	38
203	Oxygen Partial Pressure Dependence of Direct Growth of Y123 and Nd123 by Containerless Processing. Nippon Kinzoku Gakkaishi/Journal of the Japan Institute of Metals, 2002, 66, 267-273.	0.4	0
204	Direct Crystallization of Y _{3} Fe _{5} O _{12} Garnet by Containerless Solidification Processing. Materials Transactions, 2001, 42, 233-237.	1.2	9
205	Rapid solidification of Y3Al5O12 garnet from hypercooled melt. Acta Materialia, 2001, 49, 1947-1955.	7.9	39
206	Direct growth of REBa2Cu3O7-δ (RE=Yb, Er, Y, Dy, Eu, Sm, Nd and Pr) from undercooled melt using aero-acoustic levitator. Acta Materialia, 2001, 49, 2557-2565.	7.9	12
207	On occurrence of multiple-site crystallization in undercooled mullite melts. Scripta Materialia, 2001, 45, 1431-1437.	5.2	10
208	Formation of NdBa ₂ Cu ₃ O _{7â^îî} amorphous phase by combining aero-acoustic levitation and splat quenching. Journal of Materials Research, 2001, 16, 138-145.	2.6	10
209	Phase selection of peritectic phase in undercooled Nd-based superconducting oxides. Acta Materialia, 2000, 48, 3049-3057.	7.9	38
210	Peritectic Coupled Growth in Nd-Based Superconducting Oxides from Highly Undercooled Melt. Materials Science Forum, 2000, 329-330, 197-202.	0.3	0
211	Containerless Solidification of Peritectic and Eutectic Ceramics Using Aero-Acoustic Levitator. Materials Science Forum, 2000, 329-330, 173-178.	0.3	11
212	Microstructural control of NdBa2Cu3O7â^î´superconducting oxide from highly undercooled melt by containerless processing. Journal of Crystal Growth, 1999, 200, 118-125.	1.5	38
213	Grain Size Increase and Field-Effect Mobility Enhancement of Pentacene Thin Films Prepared in a Low-Pressure H ₂ Ambient. Applied Physics Express, 0, 1, 041801.	2.4	17
214	Low Temperature Phosphorus Activation in Germanium through Nickel Germanidation for Shallow n ⁺ /p Junction. Applied Physics Express, 0, 2, 021202.	2.4	28
215	Ge/GeO ₂ Interface Control with High-Pressure Oxidation for Improving Electrical Characteristics. Applied Physics Express, 0, 2, 071404.	2.4	103
216	Mobility Variations in Mono- and Multi-Layer Graphene Films. Applied Physics Express, 0, 2, 025003.	2.4	131

#	Article	IF	CITATIONS
217	Resistive Switching in NiO Bilayer Films with Different Crystallinity Layers. Key Engineering Materials, 0, 470, 188-193.	0.4	2
218	Identification of the position of piezoelectric polarization at the MoS2/metal interface. Applied Physics Express, 0, , .	2.4	0